

Circuit quantum electrodynamics with a spin qubit

K. D. Petersson¹, L. W. McFaul¹, M. D. Schroer¹, M. Jung¹, J. M. Taylor², A. A. Houck³ & J. R. Petta^{1,4}

Electron spins trapped in quantum dots have been proposed as basic building blocks of a future quantum processor^{1–3}. Although fast, 180-picosecond, two-quantum-bit (two-qubit) operations can be realized using nearest-neighbour exchange coupling⁴, a scalable, spin-based quantum computing architecture will almost certainly require long-range qubit interactions. Circuit quantum electrodynamics (cQED) allows spatially separated superconducting qubits to interact via a superconducting microwave cavity that acts as a ‘quantum bus’, making possible two-qubit entanglement and the implementation of simple quantum algorithms^{5–7}. Here we combine the cQED architecture with spin qubits by coupling an indium arsenide nanowire double quantum dot to a superconducting cavity^{8,9}. The architecture allows us to achieve a charge–cavity coupling rate of about 30 megahertz, consistent with coupling rates obtained in gallium arsenide quantum dots¹⁰. Furthermore, the strong spin–orbit interaction of indium arsenide allows us to drive spin rotations electrically with a local gate electrode, and the charge–cavity interaction provides a measurement of the resulting spin dynamics. Our results demonstrate how the cQED architecture can be used as a sensitive probe of single-spin physics and that a spin–cavity coupling rate of about one megahertz is feasible, presenting the possibility of long-range spin coupling via superconducting microwave cavities.

The weak magnetic moment of the electron makes it difficult to couple spin qubits that are separated by a large distance. Approaches to transferring spin information include physically shuttling electrons with surface acoustic waves or using exchange-coupled spin chains, both of which are experimentally challenging to realize^{11–13}. An attractive alternative for realizing long-distance spin-qubit interactions is to interface spins with a superconducting microwave cavity in the cQED architecture. Unfortunately, direct coupling between a single spin magnetic dipole and the magnetic field of the cavity results in a spin–cavity coupling rate of $g_M/2\pi \approx 10$ Hz, which is much too weak to be useful for quantum information processing¹⁴. Recent experiments have explored coupling ensembles of spins to superconducting resonators, with the large number of spins, $N_S \approx 10^{12}$, giving a $\sim N_S^{1/2}$ enhancement in the spin–cavity coupling rate^{15–17}.

Another approach to spin–cavity coupling relies on the spin–orbit interaction¹⁸. Spin–orbit coupling mixes spin and orbital degrees of freedom, resulting in spin states that have some orbital character, the spin–orbit doublets, $|\uparrow\rangle$ and $|\downarrow\rangle$. Although electron spin states cannot be coupled directly to an electric field, the spin–orbit interaction enables electrical control by perturbing the orbital component of the electron wavefunction. Fast, coherent electrical control of spin states in quantum dots has been demonstrated in InAs nanowires where the spin–orbit interaction strength is large^{8,9,19}. The cQED architecture could be used to couple two distant InAs nanowire quantum dot spin qubits with the spin–orbit interaction enabling a significantly increased spin–cavity coupling rate, g_S (ref. 18). In this Letter, we take the first steps towards realizing this approach and couple the electric field of a high-quality-factor superconducting cavity to an InAs nanowire double quantum dot (DQD) device. We determine the charge–cavity coupling rate, g_C , for the molecular orbital states of a single excess

charge in the DQD. Then, with each of the two quantum dots acting as a spin qubit, we perform fast electrical spin-state control followed by single spin read-out using the microwave cavity. Our results demonstrate that spin qubits, which require substantial magnetic fields for their operation, can be readily integrated into the superconducting cQED architecture and pave the way for long-range coupling of spin qubits via microwave cavities.

Our hybrid spin-qubit/superconducting device is shown in Fig. 1. We fabricate a half-wavelength superconducting Nb resonator (the cavity) with a resonance frequency of $f_0 = \omega_0/2\pi \approx 6.2$ GHz and quality factor of $Q \approx 2000$ (Supplementary Information, section 2). The amplitude and phase responses of the cavity are detected using a homodyne measurement with a microwave probe frequency f_R (ref. 5). We couple a single InAs nanowire spin qubit to the electric field generated by the cavity¹⁸. The qubit consists of a DQD defined in an InAs nanowire^{8,9}. A series of Ti/Au depletion gates create a simple double-well confinement potential containing (N_L, N_R) electrons, where N_L and N_R are the numbers of electrons in

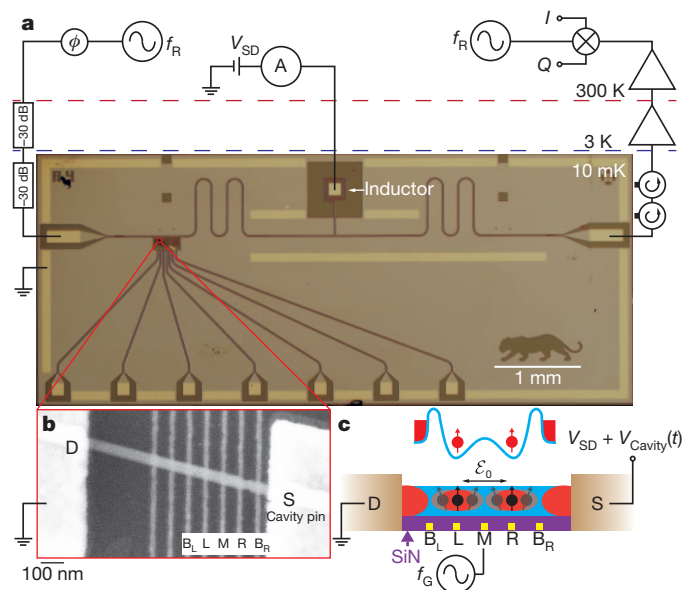


Figure 1 | Hybrid DQD/superconducting resonator device. **a**, Circuit schematic and micrograph of the hybrid device design. Transmission through the half-wavelength superconducting Nb resonator is measured using homodyne detection at a frequency f_R . Standard d.c. transport measurements are made possible by applying a source–drain bias, V_{SD} , to the DQD using a ~ 4 -nH spiral inductor that is connected to the voltage node of the resonator²³. See Supplementary Information, section 1, for further details. **b**, **c**, Scanning electron micrograph (**b**) and cross-sectional schematic view (**c**) of a typical nanowire DQD. The left and right barrier gates (B_L and B_R), left and right plunger gates (L and R), and middle gate (M) are biased to create a double-well potential within the nanowire. The drain contact of the nanowire, D , is grounded, and the source contact, S , is connected to an antinode of the resonator, oscillating at a voltage $V_{Cavity}(t)$. An a.c. voltage at a frequency f_G is applied to gate M to generate an oscillating electric field, \mathcal{E}_0 .

¹Department of Physics, Princeton University, Princeton, New Jersey 08544, USA. ²Joint Quantum Institute/NIST, College Park, Maryland 20742, USA. ³Department of Electrical Engineering, Princeton University, Princeton, New Jersey 08544, USA. ⁴Princeton Institute for the Science and Technology of Materials (PRISM), Princeton University, Princeton, New Jersey 08544, USA.

the left- and right-hand dots, respectively. We tune the tunnel coupling, t_C , of the DQD by adjusting the voltage, V_M , on the middle barrier gate (M in Fig. 1b). A trapped electron in the DQD has an electric dipole moment of $d \approx 1,000ea_0$, where a_0 is the Bohr radius and e is the electronic charge.

For a spin in a single quantum dot, the calculation in ref. 18 predicts a spin-cavity coupling rate of $g_S \approx g_C(E_Z/\Delta E_0)(l/\lambda_{SO})$, where E_Z is the Zeeman splitting of the spin states, ΔE_0 is the orbital level spacing, l is the quantum dot size and λ_{SO} is the spin-orbit length, which characterizes the strength of the spin-orbit interaction¹⁸. Therefore, strong spin-cavity coupling requires two key components: a large charge-cavity coupling rate and a strong spin-orbit interaction. Charge-cavity coupling is achieved through the electric dipole interaction, as in experiments with superconducting qubits. An oscillating electric field, with amplitude \mathcal{E}_0 , periodically displaces the electron quantum dot potential by a distance $r_0 = e\mathcal{E}_0 l^2/\Delta E_0$ (Fig. 1c), which is dependent on the quantum dot confinement as determined by ΔE_0 and l (ref. 19). To enhance the cavity electric field at the position of the DQD—and maximize the charge-cavity coupling rate—the source and drain contacts of the nanowire are connected directly to the voltage antinode and the ground of the resonator. In the presence of a strong spin-orbit interaction, the displacement of the electron can induce spin-state rotations at a rate $E_Z/\hbar \times r_0/\lambda_{SO}$, where \hbar denotes Planck's constant divided by 2π , with the linear dependence in E_Z due to the Van Vleck zero-field cancellation of the spin-orbit term. Strong spin-orbit coupling is achieved using InAs, which has a short spin-orbit length, $\lambda_{SO} \approx 100$ nm (ref. 20).

We first characterize the interaction between an electron trapped in a DQD and the electric field of the cavity, demonstrating a 30-MHz charge-cavity coupling rate with this device architecture. We focus on the cavity response near the $(M, N+1) \leftrightarrow (M+1, N)$ interdot charge transition in the many-electron regime ($M \approx 20, N \approx 20$; Supplementary Information, section 3). The DQD forms a two-level 'artificial molecule' with an energy splitting of $\Omega = \sqrt{\varepsilon^2 + 4t_C^2}$, where ε is the detuning (Fig. 2a, top). Interdot tunnel coupling hybridizes the charge states around $\varepsilon = 0$, resulting in a tunnel splitting of $2t_C$. The detuning-dependent dipole moment of the DQD has an admittance that loads the cavity. We characterize the strength of the interaction by the a.c. susceptibility, χ (ref. 21; Fig. 2a, bottom).

A qualitative understanding of the coupling between the quantum dot and the cavity can be obtained by considering the relevant energy scales in the system. The single-dot charging energy, $E_C \approx 12$ meV, is much larger than the relevant photon energy, $\hbar f_R \approx 25$ μ eV, and the cavity is largely unaffected by the DQD in Coulomb blockade. However, near interdot charge transitions (for example $(M, N+1) \leftrightarrow (M+1, N)$) or transitions with the source and drain electrodes (for example $(M, N) \leftrightarrow (M, N+1)$), the energy scales associated with the DQD are close to the cavity energy, and the cavity is damped, resulting in a phase shift in microwave transmission at the bare cavity frequency. In Fig. 2b, the DQD charge stability diagram is measured around the $(M, N+1) \leftrightarrow (M+1, N)$ transition by probing the phase response of the microwave cavity as a function of the gate voltages V_L and V_R (refs 10, 22).

Quantitative analysis of the cavity response requires a fully quantum mechanical model that accounts for photon exchange between the microwave field and the DQD^{18,23}. In cavity QED, the pertinent interactions are those between an atom with transition frequency $\omega_a = \Omega/\hbar$ and the photon field of the cavity, characterized by the resonance frequency ω_0 . The atom and cavity energy levels hybridize when the atom-cavity detuning, $\Delta = \omega_a - \omega_0$, is less than g_C , leading to the Jaynes-Cummings ladder of quantum states²⁴. When the atom and cavity are detuned in the dispersive limit ($\Delta > g_C$), the cavity field exhibits a phase shift in microwave transmission at the bare cavity frequency that is given by $\phi = -\arctan(2g_C^2/\kappa\Delta)$, where κ is the cavity decay rate. In Fig. 2d, we plot the phase response of the cavity for several values of the interdot tunnel coupling (see Supplementary

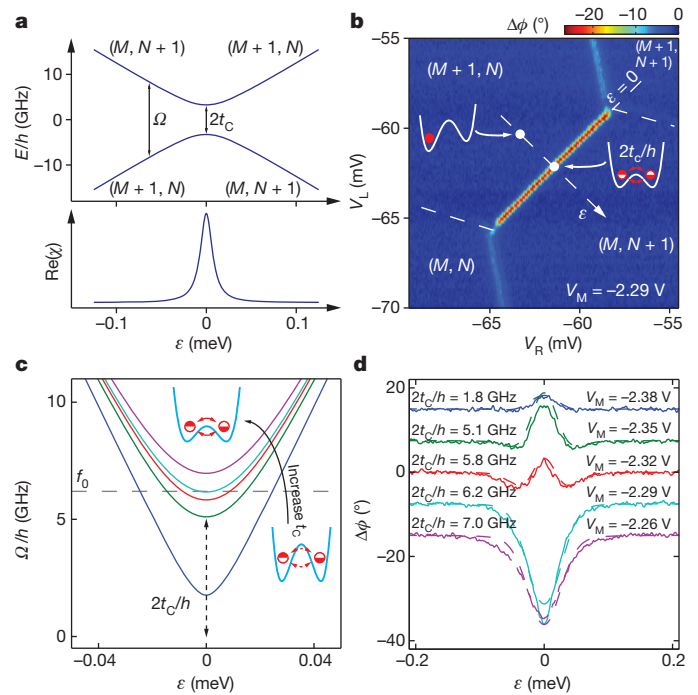


Figure 2 | Measurement of the DQD charge-cavity coupling. **a**, DQD energy levels (top) and a.c. susceptibility, χ (bottom), as functions of detuning, ε . **b**, Phase response of the cavity as a function of gate voltages V_L and V_R near the $(M+1, N) \leftrightarrow (M, N+1)$ charge transition, measured using a fixed drive frequency, $f_R = 6194.8$ MHz. The dashed arrow indicates the detuning axis. At the interdot charge transition ($\varepsilon = 0$) an excess electron is delocalized across the DQD. Away from zero detuning, the electron is trapped in one of the dots. **c**, Cavity frequency, f_0 (approximately constant at 6.2 GHz), relative to the bare qubit transition frequency, Ω/h , for different values of the interdot tunnel coupling, t_C , as extracted from the data in **d**. **d**, Phase response measured as a function of DQD detuning, ε , for a range of tunnel couplings, t_C , as set by V_M . The detuning is varied by sweeping V_R . Phase data are offset by 7.5° for clarity. Dashed lines are fits to the data, allowing the determination of the charge-cavity coupling rate, $g_C/2\pi \approx 30$ MHz (see main text).

Information, section 4 for the magnitude response). We observe a sign change in the phase as the atom-cavity detuning, Δ , is varied from positive to negative values⁵. We fit the phase and magnitude data to a master equation model (Supplementary Information, section 6.1) using a best-fit value of $g_C/2\pi = 30$ MHz; an inhomogeneous broadening parameter, $\sigma_e/h = 5.1$ GHz, to account for low-frequency charge noise; and a V_M -dependent tunnel coupling that ranges from $2t_C/h = 1.8$ to 7.0 GHz (Fig. 2c). The charge-cavity coupling rate extracted here compares favourably to values obtained using Cooper pair box qubits⁵ ($g_C/2\pi \approx 6$ MHz), transmon qubits²⁵ ($g_C/2\pi \approx 100$ MHz) and many-electron GaAs quantum dots¹⁰ ($g_C/2\pi \approx 50$ MHz).

We characterize the strength of the spin-orbit interaction by operating the device as a spin qubit (Fig. 3). For simplicity, we label the charge states $(1, 1)$ and $(0, 2)$ (ref. 4). The ground state with two electrons in the right quantum dot is the singlet $S(0, 2)$. At negative detuning, the electrons are separated in a $(1, 1)$ charge state, and the four relevant spin states are $|\uparrow\uparrow\rangle$, $|\downarrow\downarrow\rangle$, $|\uparrow\downarrow\rangle$ and $|\downarrow\uparrow\rangle$ (ref. 8). The level diagram is similar to a GaAs singlet-triplet spin qubit, with a key difference being that the g -factors for the two spins can vary significantly⁴ (Supplementary Information, section 6.2). Interdot tunnel coupling hybridizes the states with singlet character near $\varepsilon = 0$, and an external field results in Zeeman splitting, $E_Z = \tilde{g}\mu_B B$, of the spin states, where \tilde{g} is the electronic g -factor, μ_B is the Bohr magneton and B is the magnetic field.

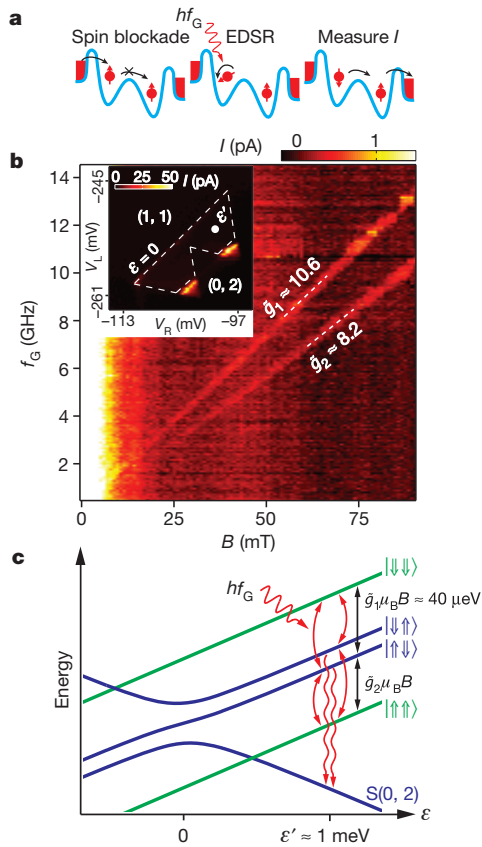


Figure 3 | Spin-qubit spectroscopy. **a**, The measurement cycle for spin-qubit spectroscopy. The DQD is put in either the $|\uparrow\uparrow\rangle$ or the $|\downarrow\downarrow\rangle$ spin configuration as a result of Pauli spin blockade. EDSR transitions lift this blockade, resulting in current flow through the device. **b**, Spin-qubit spectroscopy as a function of magnetic field, B , measured under Pauli blockade. Pauli blockade is lifted by EDSR driving when the microwave frequency is $f_G = \tilde{g}_i \mu_B B / h$, where \tilde{g}_i ($i = 1, 2$) is the electronic g -factor of dot i . Inset, current through the DQD as a function of gate voltages V_L and V_R , with $V_{SD} = 2.5$ mV. Current is suppressed inside the dashed region owing to Pauli spin blockade. **c**, Energy levels of the spin-orbit qubit plotted as a function of ε . The data in **b** are acquired with $\varepsilon = \varepsilon' \approx 1$ meV.

Spin selection rules result in Pauli blockade at the two-electron transition, a key ingredient for spin preparation and measurement^{4,8,26} (Fig. 3b, inset). For example, state $|\uparrow\uparrow\rangle$ cannot tunnel to $S(0, 2)$ due to Pauli exclusion. Modulation of the confinement potential with a gate voltage results in spin-orbit-driven electric dipole spin resonance (EDSR) transitions that lift the Pauli blockade^{8,19}. In Fig. 3b, we plot the current, I , through the DQD with $V_{SD} = 2.5$ meV and the gates tuned in Pauli blockade (Fig. 3b, white dot in inset). Hyperfine fields rapidly mix spin states when $E_Z = \tilde{g}_i \mu_B B < B_N$, where $B_N \approx 2$ mT is the hyperfine field⁹. At finite fields, the leakage current is non-zero when the a.c. driving frequency on the gate, f_G , satisfies the electron spin resonance condition $E_Z = hf_G$. We observe two resonance conditions corresponding to single spin rotations in the left- and right-hand quantum dots, with g -factors of 8.2 and 10.6 (ref. 8).

In cQED with superconducting qubits, measurements of the cavity response can be used for qubit read-out. For spin qubits, around $\varepsilon = 0$, the DQD has a spin-state-dependent dipole moment due to Pauli blockade that allows spin-state read-out via the superconducting cavity²⁷. We combine quantum control of the spins using EDSR and cavity detection of single-spin dynamics using the pulse sequence shown in Fig. 4a, b. Starting with the spin qubit in state $|\uparrow\uparrow\rangle$, we pulse to negative detuning ($\varepsilon = \varepsilon' \approx -2$ meV) and apply a microwave burst of length τ_B to drive EDSR transitions. For example, an EDSR π -pulse will drive a spin transition from $|\uparrow\uparrow\rangle$ to $|\downarrow\downarrow\rangle$. The resulting spin state is probed by

pulsing back to $\varepsilon = 0$ for a measurement time T_M . The cavity is most sensitive to charge dynamics near $\varepsilon = 0$ owing to the different a.c. susceptibilities of spin states $|\downarrow\downarrow\rangle$ and $|\uparrow\uparrow\rangle$ (Supplementary Information, section 6.3). In Fig. 4c, we plot the cavity phase shift as a function of f_G and B . We again observe two features that follow the standard spin resonance condition, consistent with the d.c. transport data in Fig. 4b. By varying T_M , we fit the measured phase response to theory and estimate a spin lifetime of $T_1 \approx 1$ μ s (Fig. 4d). We anticipate that the relaxation time is detuning dependent, with longer spin relaxation times away from $\varepsilon = 0$ (ref. 28; Supplementary Information, section 5).

We demonstrate coherent control of the spin qubit and read-out via the cavity by varying the EDSR microwave burst length, τ_B . Figure 4e

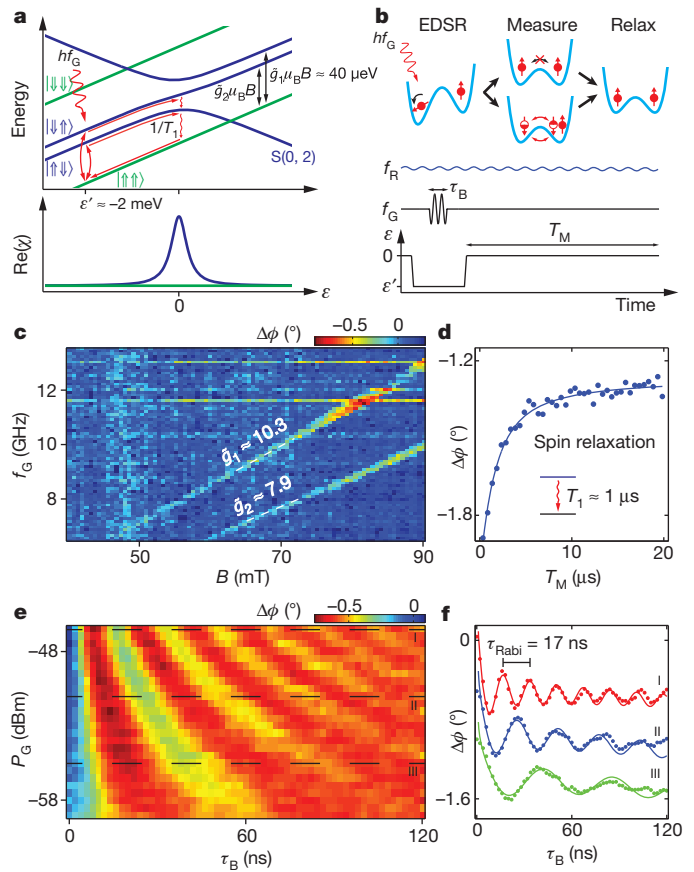


Figure 4 | Coherent spin-state control and detection using the microwave cavity. **a**, Top: pulse sequence used for spin-state control and resonator read-out, superimposed on the level diagram. Bottom: the a.c. susceptibility, χ , is dependent on the spin state of the DQD and allows for sensitive spin read-out via the microwave cavity. **b**, Pulse sequence used for spin-state control and resonator read-out. Starting in state $|\uparrow\uparrow\rangle$, an EDSR burst is applied at far detuning ($\varepsilon = \varepsilon' \approx -2$ meV) and the resultant spin state is then measured at $\varepsilon = 0$ by probing the cavity transmission using a weak continuous tone of frequency f_R . **c**, Phase response of the cavity measured as a function of EDSR drive frequency, f_G , and external field, B , with $\tau_B = 100$ ns and $T_M = 850$ ns. EDSR transitions are observed in the phase response, in agreement with the d.c. transport data, with small differences in \tilde{g}_1 and \tilde{g}_2 attributable to the difference in sample tuning necessary to optimize the response. **d**, Measured phase shift as a function of T_M , with $\tau_B = 100$ ns, $B = 90$ mT and $f_G = 13.1$ GHz. A fit to theory yields a spin relaxation time of $T_1 = 1$ μ s. **e**, Phase response of the cavity as a function of EDSR burst length, τ_B , and approximate driving power at the sample, P_G , for $B = 86$ mT, $f_G = 9.5$ GHz and $T_M = 1.75$ μ s. Data were taken at a different sample tuning from data in **c–d**. **f**, Rabi oscillations at different powers, indicated by the dashed lines in **e**. The data are shifted in phase by 0.45° for clarity. The solid curves are fits to a power-law decay. We obtain a minimum Rabi period of $\tau_{\text{Rabi}} = 17$ ns (Supplementary Information, section 5).

shows the measured phase as a function of τ_B and the gate drive power, P_G . We observe Rabi oscillations with a minimum period of 17 ns (Fig. 4f), consistent with an EDSR driving mechanism⁸. These data show how the microwave field of the cavity is sensitive to the spin state of a single electron and that by using the cQED architecture quantum dot spin states may be coherently controlled and measured using microwave electric fields.

Long-distance coupling of spin qubits via a cavity will require a spin-cavity coupling rate that is larger than the cavity decay rate and the qubit decoherence rate. Although the method of spin-state readout that we have demonstrated does not imply spin-cavity coupling, on the basis of our results we can estimate the effective spin-cavity coupling strength. From our measurements, we find that $g_C/2\pi = 30$ MHz, $E_Z = 25$ μ eV and $\Delta E_0 = 1.7$ meV, which gives $l = \hbar / \sqrt{m^* \Delta E_0} \approx 40$ nm, where m^* , the effective electron mass in InAs, is 0.023 times the bare electron mass. Assuming a spin-orbit length of $\lambda_{SO} \approx 100$ nm (ref. 20), we find a spin-cavity coupling rate of $g_S/2\pi \approx 0.2$ MHz, which is four orders of magnitude larger than the coupling rate g_M that would be obtained by coupling a single spin to the magnetic field of a microwave cavity. This spin-cavity coupling rate could be readily increased to ~ 1 MHz by increasing the cavity resonance frequency to $f_0 = 15$ GHz (which would proportionally increase both g_C and E_Z). Recent theoretical work also predicts an enhanced spin-cavity coupling for a single spin in a DQD biased at $\varepsilon = 0$ (ref. 29).

In addition to increasing the spin-cavity coupling rate, there is significant scope for improving the cavity decay rate and the qubit decoherence rate. Optimization of the resonator design will reduce the cavity decay rate to well below 1 MHz (Supplementary Information, section 2). There are several options for decreasing the qubit decoherence rate, which is at present limited by coupling to the nuclear spin bath. Dynamical decoupling has already been used to reduce the qubit decay rate to ~ 1 MHz in the InAs system⁸. InAs could also be replaced by nuclear-spin-free Ge/Si core-shell nanowires where hole spin-orbit coupling is predicted to be large³⁰. On the basis of our results, we anticipate that the strong-coupling regime for single spins can be reached, eventually allowing spin qubits to be interconnected in a quantum bus architecture.

METHODS SUMMARY

Samples were fabricated on high-resistivity, (100)-orientation silicon wafers with 250 nm of dry thermal oxide. Superconducting resonators were formed by first sputter-depositing a 100-nm-thick Nb layer followed by a 30-nm Au film without breaking vacuum. The Au film was removed, except in regions that were later contacted by either wire bonds or electron-beam lithography (EBL), by a chemical wet etch in a solution of hydrochloric acid and nitric acid. A half-wavelength resonator was defined using photolithography followed by etching in a solution of hydrofluoric acid and nitric acid. Bottom gate electrode arrays were then patterned using EBL as described in further detail elsewhere^{8,9}. A ~ 26 -nm-thick layer of SiNx was deposited on top of the gate electrodes using plasma-enhanced chemical vapour deposition with the Nb film protected with photoresist, followed by lift-off and then further patterning using EBL and reactive ion etching. InAs nanowires were then dispersed from an ethanol solution, located using optical microscopy, and contacted using EBL.

The microwave response was measured using homodyne detection. A resonator tone with frequency f_R was applied through heavily attenuated, semi-rigid coaxial cables. The transmitted signal was first passed through two stages of isolators and then amplified using a ~ 3 K cryogenic amplifier. Room-temperature (~ 300 K) amplifiers provided additional gain of 55 dB, before the signal was demodulated using an IQ mixer. Following further amplification and filtering, we recorded the in-phase (I) and quadrature (Q) components to extract the amplitude and phase of the transmitted microwave signal. The EDSR microwave drive was provided by a vector microwave source, and detuning pulses were generated by an arbitrary-waveform generator. These were combined and coupled to gate M through an attenuated semi-rigid coaxial cable and a bias tee at the sample holder. The waveform generator also controlled the timing of the EDSR microwave bursts.

Received 4 June; accepted 24 August 2012.

- Loss, D. & DiVincenzo, D. P. Quantum computation with quantum dots. *Phys. Rev. A* **57**, 120–126 (1998).
- Koppens, F. H. L. *et al.* Driven coherent oscillations of a single electron spin in a quantum dot. *Nature* **442**, 766–771 (2006).
- Hanson, R., Kouwenhoven, L. P., Petta, J. R., Tarucha, S. & Vandersypen, L. M. K. Spins in few-electron quantum dots. *Rev. Mod. Phys.* **79**, 1217–1265 (2007).
- Petta, J. R. *et al.* Coherent manipulation of coupled electron spins in semiconductor quantum dots. *Science* **309**, 2180–2184 (2005).
- Wallraff, A. *et al.* Strong coupling of a single photon to a superconducting qubit using circuit quantum electrodynamics. *Nature* **431**, 162–167 (2004).
- Reed, M. D. *et al.* Realization of three-qubit quantum error correction with superconducting circuits. *Nature* **482**, 382–385 (2012).
- Sillanpää, M. A., Park, J. I. & Simmonds, R. W. Coherent quantum state storage and transfer between two phase qubits via a resonant cavity. *Nature* **449**, 438–442 (2007).
- Nadj-Perge, S., Frolov, S. M., Bakkers, E. & Kouwenhoven, L. P. Spin-orbit qubit in a semiconductor nanowire. *Nature* **468**, 1084–1087 (2010).
- Schroer, M. D., Petersson, K. D., Jung, M. & Petta, J. R. Field tuning the g factor in InAs nanowire double quantum dots. *Phys. Rev. Lett.* **107**, 176811 (2011).
- Frey, T. *et al.* Dipole coupling of a double quantum dot to a microwave resonator. *Phys. Rev. Lett.* **108**, 046807 (2012).
- Hermelin, S. *et al.* Electrons surfing on a sound wave as a platform for quantum optics with flying electrons. *Nature* **477**, 435–438 (2011).
- McNeil, R. P. G. *et al.* On-demand single-electron transfer between distant quantum dots. *Nature* **477**, 439–442 (2011).
- Friesen, M., Biswas, A., Hu, X. & Lidar, D. Efficient multiqubit entanglement via a spin bus. *Phys. Rev. Lett.* **98**, 230503 (2007).
- Imamoğlu, A. Cavity QED based on collective magnetic dipole coupling: spin ensembles as hybrid two-level systems. *Phys. Rev. Lett.* **102**, 083602 (2009).
- Schuster, D. I. *et al.* High-cooperativity coupling of electron-spin ensembles to superconducting cavities. *Phys. Rev. Lett.* **105**, 140501 (2010).
- Kubo, Y. *et al.* Hybrid quantum circuit with a superconducting qubit coupled to a spin ensemble. *Phys. Rev. Lett.* **107**, 220501 (2011).
- Amsüss, R. *et al.* Cavity QED with magnetically coupled collective spin states. *Phys. Rev. Lett.* **107**, 060502 (2011).
- Trif, M., Golovach, V. N. & Loss, D. Spin dynamics in InAs nanowire quantum dots coupled to a transmission line. *Phys. Rev. B* **77**, 045434 (2008).
- Golovach, V. N., Borhani, M. & Loss, D. Electric-dipole-induced spin resonance in quantum dots. *Phys. Rev. B* **74**, 165319 (2006).
- Fasth, C., Fuhrer, A., Samuelson, L. G., Vityay, N. & Loss, D. Direct measurement of the spin-orbit interaction in a two-electron InAs nanowire quantum dot. *Phys. Rev. Lett.* **98**, 266801 (2007).
- Blais, A., Huang, R. S., Wallraff, A., Girvin, S. M. & Schoelkopf, R. J. Cavity quantum electrodynamics for superconducting electrical circuits: an architecture for quantum computation. *Phys. Rev. A* **69**, 062320 (2004).
- Delbecq, M. R. *et al.* Coupling a quantum dot, fermionic leads, and a microwave cavity on a chip. *Phys. Rev. Lett.* **107**, 256804 (2011).
- Chen, F., Sirois, A. J., Simmonds, R. W. & Rimberg, A. J. Introduction of a dc bias into a high-Q superconducting microwave cavity. *Appl. Phys. Lett.* **98**, 132509 (2011).
- Jaynes, E. T. & Cummings, F. W. Comparison of quantum and semiclassical radiation theories with application to the beam maser. *Proc. IEEE* **51**, 89–109 (1963).
- Schuster, D. I. *et al.* Resolving photon number states in a superconducting circuit. *Nature* **445**, 515–518 (2007).
- Ono, K., Austing, D. G., Tokura, Y. & Tarucha, S. Current rectification by Pauli exclusion in a weakly coupled double quantum dot system. *Science* **297**, 1313–1317 (2002).
- Petersson, K. D. *et al.* Charge and spin state readout of a double quantum dot coupled to a resonator. *Nano Lett.* **10**, 2789–2793 (2010).
- Johnson, A. C. *et al.* Triplet-singlet spin relaxation via nuclei in a double quantum dot. *Nature* **435**, 925–928 (2005).
- Hu, X., Lu, Y. & Nori, F. Strong coupling of a spin qubit to a superconducting stripline cavity. *Phys. Rev. B* **86**, 035314 (2012).
- Kloeffel, C., Trif, M. & Loss, D. Strong spin-orbit interaction and helical hole states in Ge/Si nanowires. *Phys. Rev. B* **84**, 195314 (2011).

Supplementary Information is available in the online version of the paper.

Acknowledgements Research at Princeton University was supported by the Alfred P. Sloan Foundation, the David and Lucile Packard Foundation, US Army Research Office grant W911NF-08-1-0189, DARPA QuEST award HRO011-09-1-0007 and the US National Science Foundation through the Princeton Center for Complex Materials (DMR-0819860) and CAREER award DMR-0846341. J.M.T. acknowledges support from ARO MURI award W911NF-09-1-0406.

Author Contributions K.D.P. fabricated the sample and performed the measurements. K.D.P., L.W.M. and A.A.H. developed the resonator fabrication and measurement processes. K.D.P., M.D.S. and M.J. developed the nanowire device fabrication processes. M.D.S. grew the nanowires. J.M.T. developed the theory for the experiment. K.D.P. and J.R.P. wrote the paper with input from the other authors. J.R.P. planned the experiment.

Author Information Reprints and permissions information is available at www.nature.com/reprints. The authors declare no competing financial interests. Readers are welcome to comment on the online version of the paper. Correspondence and requests for materials should be addressed to J.R.P. (petta@princeton.edu).